Air gun with water bullet

Zafer Bozkuş [1], Ali Ersin Dinçer [2], Arris S. Tijsseling [3] and Fons van de Ven [3]

[1] Hydraulics Lab., Dept. of Civil Engineering, Middle East Technical University, 06800, Çankaya/Ankara, Turkey. E-mail: bozkus@metu.edu.tr

[2] Dept. of Civil Engineering, Abdullah Gul University, Barbaros, Sümer Kampüsü, Erkilet Blv., 38080 Kocasinan/Kayseri, Turkey. E-mail: ersin.dincer@agu.edu.tr

[3] Department of Mathematics and Computer Science, Eindhoven University of Technology, P.O. Box 513, 5600 MB Eindhoven, The Netherlands. E-mails: a.s.tijsseling@tue.nl (corresponding author); a.a.f.v.d.ven@tue.nl

ABSTRACT

The gun is a 12 m long inclined pipe of 0.1 m diameter which is connected to a charge of compressed air contained in a 0.5 m^3 vessel. The bullet is a slug of water sitting in the upstream lower end of the pipe. The trigger is a hand-operated valve. The target is an elbow at the upstream higher end of the pipe. The smoking gun effect is created by a mist of water coming out of the pipe after each shot. The apparatus is not a toy but meant for serious research. When steam lines are out of operation and/or lack thermal insulation, liquid water collects in the lower parts of the system. System restart may accelerate the water slugs to velocities as high as 50 m/s, and subsequent slug impacts on elbows and orifices may cause pressure peaks with magnitudes only encountered in water-hammer events. The experimental programme consists of water slugs fired towards an elbow with an open end, a closed end, and an orifice end. The varied parameters are air pressure, water mass, outlet condition (open, closed, orifice). Upstream driving pressure and downstream impact pressure are measured in each experimental run. Pressure peaks up to 50 bar have been observed. Experimental results are compared with preliminary predictions from basic one-dimensional models.

Keywords liquid slug impact, entrapped gas pocket, air hammer, venting orifice, pressure transducer drifting, pressure signal reconstruction, experiment, 1D model

1 INTRODUCTION

Bullet-like individual liquid slugs travelling in an initially voided line may be the culprits for adverse conditions in pipe systems. These slugs may accelerate and attain very high speeds and cause extensive damage to pipe anchors or pipe elements when they hit obstructions like partially open valves, bends, elbows, orifices, etc. In order to prevent failure of the pipes and assure a safe operation, impact pressures due to liquid slugs should

be predicted as accurately as possible at the design stage. Design engineers run into this problem especially in thermal power plants where steam turbines are used.

Steam in the lower elevations of the pipelines may condense due to insufficient insulation resulting in the formation of liquid slugs. If the lines were not drained properly in advance, these liquid slugs are brought into motion in the next operation, and they may accelerate in the regions where driving pressures are high. Moving like a bullet in an empty pipe, it is a matter of instant before a liquid slug impacts on a pipe element. Another practical example is the acceleration of a water slug into an open air/vacuum valve that is exhausting air from a pipeline and the subsequent impact of said water slug upon the closed air/vacuum valve when the air is fully vented.

Researchers have studied impact peak pressures due to liquid slugs numerically and experimentally. The most notable experimental studies were conducted by Hashimoto et al. (1988), Fenton and Griffith (1990), Bozkuş (1991), Owen and Hussein (1994), and Bozkuş et al. (2004). Numerical models have been developed using these experimental works by (Yang and Wiggert, 1998; Kayhan and Bozkuş, 2011; Hou et al., 2014; Tijsseling et al, 2016a; Korzilius et al., 2017; Dinçer, 2017; Dinçer et al., 2018). Vasconcelos and Leite (2012) and Hatcher and Vasconcelos (2017) published related work motivated by issues in storm-water tunnels.

In the previous experimental studies of Bozkuş et al. (2004), the accelerated slug hits the elbow and leaves the pipe that is fully open to the atmosphere. The main novelty in the present study is that, in addition to the fully open case, two more configurations, a completely closed elbow and an orifice of varying diameters, are installed at the pipe end. In the next section, the experimental phase is explained in detail. Hashimoto et al. (1988) carried out a similar and most complete investigation. However, their test rig was at a smaller scale (pipes of 7.5 and 17.0 mm diameter and liquid slugs of 0.03 to 0.20 kg) and without a downstream bend. They measured upstream and downstream pressures, and the average velocity of the liquid slugs.

2 EXPERIMENTAL SETUP AND EXPERIMENT RESULTS

The experiments have been conducted in the Hydraulics Laboratory of the Civil Engineering Department at the Middle East Technical University. The sketch of the experimental setup is shown in Figure 1. The setup consists of an upstream cylindrical air tank with a volume of 0.5 m^3, a 10 cm diameter ball valve, a vertical pipe of 0.85 m length, a 12 m long upward sloped steel pipe with a 10 cm inside diameter and an angle of 4.6 degrees with respect to the horizontal plane and an elbow (mitre bend) at the end. The length of the vertical section downstream of the elbow is 0.54 m. The volume of the pipe from tank to outlet is about 0.1 m^3. The air tank is filled with pressurized air and the pipe segment just downstream of the valve is partially filled with water of known mass to form trapped liquid, i.e., a slug of desired mass. By quickly opening the ball valve, the slug is fired. During its motion it accelerates in the pipe and eventually hits the downstream elbow.

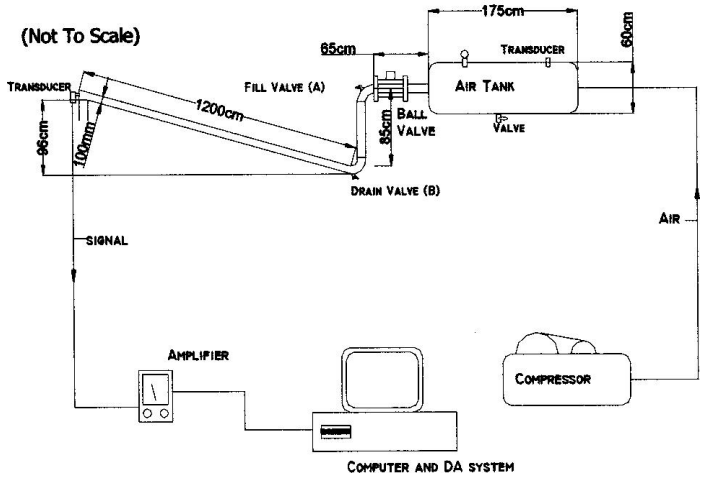

Figure 1. Illustration of experimental setup

A pressure transducer is located at the elbow to measure time variation of the impact pressure (Figure 2a), a second transducer is located upstream on the 85 cm long vertical pipe to measure the driving pressure (Figure 2b). A computer equipped with a high-speed A/D converter collects the impact data.

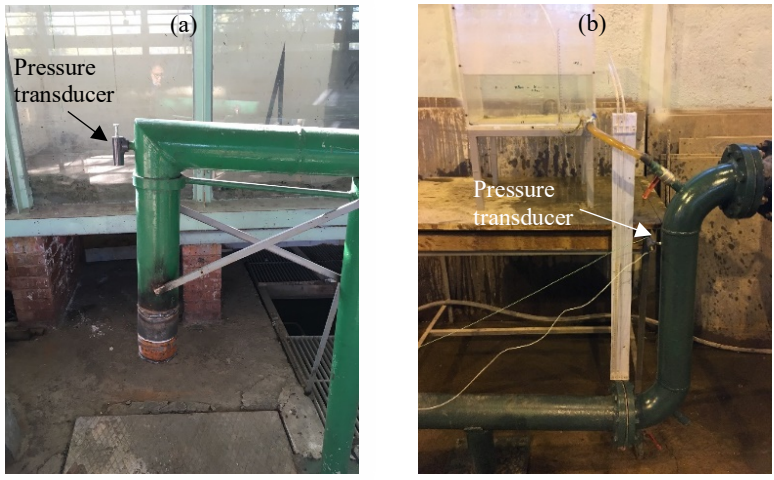

Figure 2. (a) Transducer at downstream elbow and (b) Transducer at upstream end

2.1 Description of test procedure and the pressure transducers used

As described in detail by Bozkuş et al. (2004), a typical test was performed as follows:

1) The test section of the pipe was filled with a desired mass of the water. Figure 2(b) shows the water container and the hose connection to the pipe for filling.

2) Air from the compressor was fed into the air tank until the desired initial pressure value was obtained while the ball valve was in closed position. Then, the compressor was shut off and disconnected from the air tank.

3) The ball valve was opened quickly by hand. Typically, it took about 16 ms to open the ball valve all the way. This is the average value based on several tries measured with a computer previously with the help of an accelerometer placed on the valve handle. The opening of the valve was performed in a very consistent manner so that it did not introduce additional uncertainty into the problem.

4) The pressure was recorded at the elbow with a PCB piezoelectric pressure transducer interfaced to the data acquisition system, DAS.

Most of the time the sampling rate of the DAS was 2000 Hertz. The combined uncertainty in the transient pressure measurements at the elbow was estimated to be ±12 kPa for a 500 kPa reading (0 bias, 0.95 probability). The principle of a piezoelectric transducer is that a charge is produced across the piezoelectric crystal, which is proportional to the applied pressure. Since this type of transducer is designed to measure dynamic and short-term static pressure measurements, all pressure readings taken correspond to dynamic pressure variations about a steady state static pressure. From the calibration data of the pressure transducer provided by the manufacturer, the following electronic information is available: discharge time constant $TC \geq 50$ sec, rise-time < 1μsec, natural frequency = 500 kHz, sensitivity = 9.59 mV/psi, linearity < 1.0% FS. For this study, PCB Piezotronics Model 111A26 dynamic pressure transducers with built-in unity-gain voltage-amplifiers were used. These units were selected because of their high resonance frequency, acceleration-compensated quartz element, and the fact that the signal quality is almost independent of cable length and motion. The calibration procedure as supplied by the manufacturer is in compliance with ISO 10012-1, and former MIL-STD-45662A. Moreover, these units can be used for measuring dynamic pressures of both liquids and air/gas mediums accurately.

Connected to the pressure transducer was a PCB battery power unit. The unit used was PCB Model 480E09 with 1, 10, and 100 range signal amplifiers. The function of the battery power unit is to power (by DC current) the transducer electronics, amplify the signal, remove bias from the output signal and indicate normal or faulty system operation. It is a combination of power supply and signal amplifier. As to the possible adverse effect of the pressure measurement system, i.e., transducer with connecting pressure line (water-filled cavity) on the time response of the measurements, the authors are confident that the casing arrangement was well designed and did not introduce any significant adverse effect in the measurements. This confidence is justified by the comparisons made with the results of the first author's research, Bozkuş (1991), in which the transducer at the elbow was mounted in the axial flow direction without any casing arrangement. Dynamic pressure measurements performed on both studies showed a very similar trend, indicating there was no data loss.

Notwithstanding the above, there were issues with the pressures measured in the closed-end and orifice-end tests. This matter is discussed in detail in the Appendix.

2.2 Experiments with water slugs fired towards the elbow with an open end

For comparison purposes, some of the measured pressure-time histories at the elbow are presented in Figures 3 and 4 for the fully open-end case for a liquid mass of 24 kg, with driving air pressures (gauge) of $P_{tank} = 3$ and 6 bar, respectively. As expected, the higher air pressure generates a higher (about two times) impact pressure for the same slug mass. The duration of both impacts is about 1 sec. The order of magnitude of the pressure peaks is tens of bar.

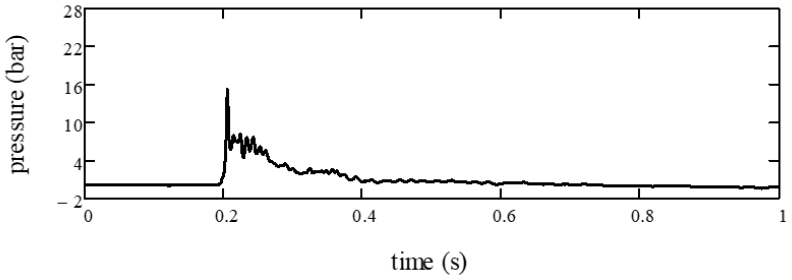

Figure 3. Pressure vs. time at elbow for 24 kg slug (P_{tank} = 3 bar, fully open pipe)

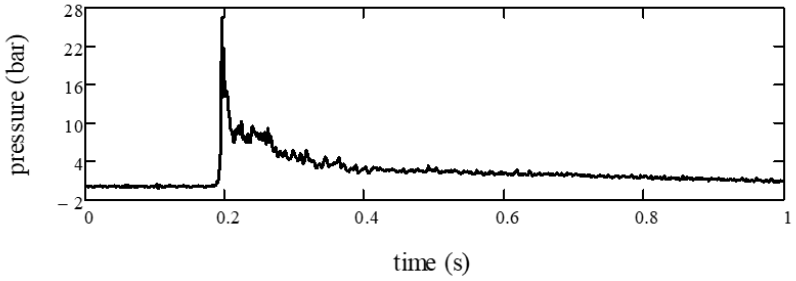

Figure 4. Pressure vs. time at elbow for 24 kg slug (P_{tank} = 6 bar, fully open pipe)

2.3 Experiments with water slugs fired towards the elbow with a closed end

Two selected figures are presented below for the closed-end situation at the elbow. Figure 5 shows the pressure trace at the elbow for a slug of 24 kg with an initial air-tank pressure of 3 bar, whereas in Figure 6 it is given for a slug of 69 kg. It is obvious in these figures that the pressure variation is drastically different from and much lower than the fully open case shown in Figures 3 and 4. The effect of trapped air between the closed end and the incoming liquid slug is generating an interesting behaviour with fluctuations as a result of the (air) spring - (liquid) mass effect. The duration of the transient event is about 1 sec.

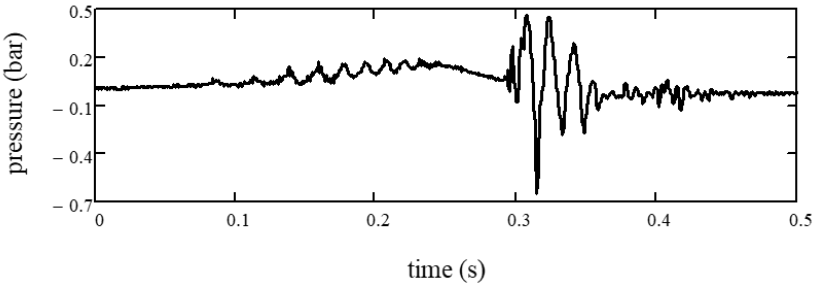

Figure 5. Pressure vs. time at elbow for 24 kg slug (P_{tank} = 3 bar, closed end)

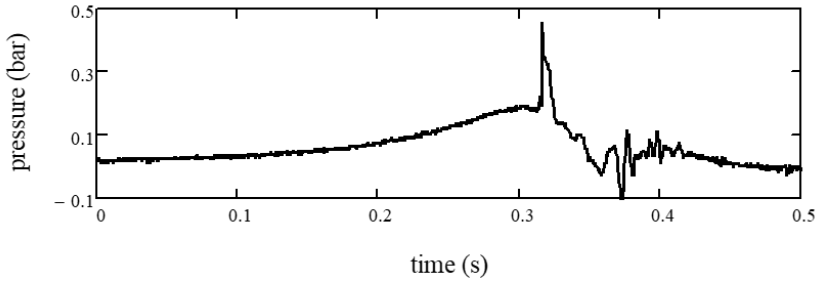

Figure 6. Pressure vs. time at elbow for 69 kg slug (P_{tank} = 3 bar, closed end)

2.4 Experiments with water slugs fired towards the elbow with an orifice end

Figures 7 and 8 show for a slug of 24 kg mass the impact pressure variation at the elbow which is closed by an end cap with an orifice of 10 mm diameter in its centre for initial tank pressures of 3 and 6 bar, respectively. Similar information is provided in Figures 9 and 10 for an orifice of 5 mm diameter. Figure 11 shows the orifices used in the experiments. The magnitudes of the pressure peaks are in between those obtained in the closed-end and open-end cases. It is evident that higher tank pressures create higher impacts (about two times for the 10 mm orifice and about five times for the 5 mm orifice) at the elbow as expected. On the other hand, when the orifice diameter is decreased from 10 mm to 5 mm, the impact pressure magnitude decreases for P_{tank} = 3 bar while it increases slightly for P_{tank} = 6 bar. The duration of the pressure oscillation is about 2 sec.

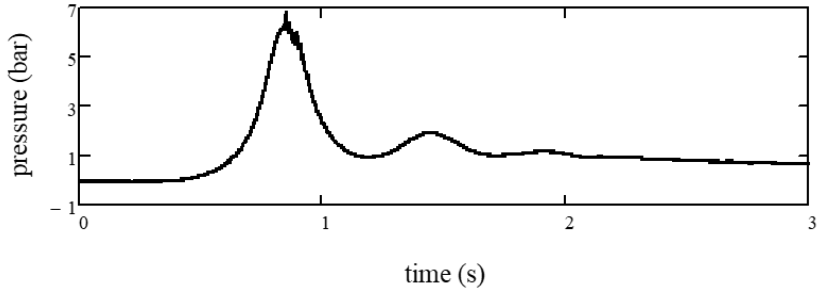

Figure 7. Pressure vs. time at elbow for 24 kg slug (P_{tank} = 3 bar, orifice D_0 = 10 mm)

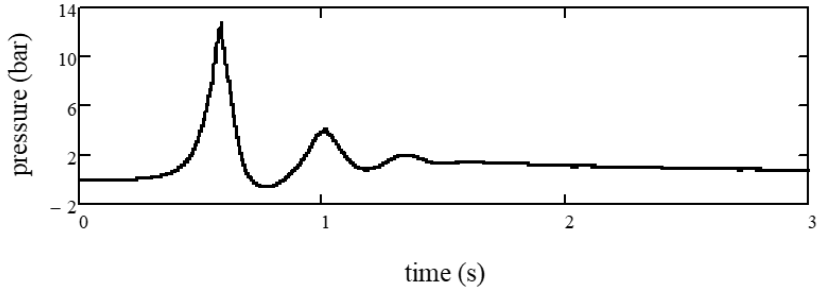

Figure 8. Pressure vs. time at elbow for 24 kg slug (P_{tank} = 6 bar, orifice D_0 = 10 mm)

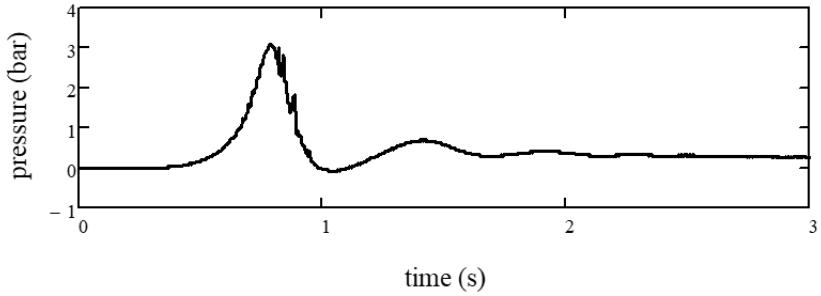

Figure 9. Pressure vs. time at elbow for 24 kg slug (P_{tank} = 3 bar, orifice D_0 = 5 mm)

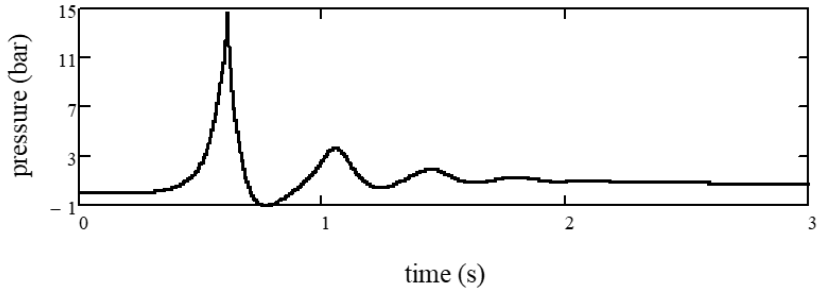

Figure 10. Pressure vs. time at elbow for 24 kg slug (P_{tank} = 6 bar, orifice D_0 = 5 mm)

Figure 11. Orifice plates (end caps) with D_0 = 10 mm (left) and 5 mm (right) diameters

3 1-D MODELS

The first and third author have developed a range of one-dimensional rigid-column models describing pipe filling, pipe emptying and travelling liquid slugs. These models are used herein solely to interpret the measured data. The derivation of the models and the solution of the governing equations are not part of this paper. The models have been kept as simple as possible: the liquid slug is a rigid mass (piston) and all compressibility is in the massless gas pocket (or column).

Open end

For liquid slugs hitting an open elbow the reader is referred to Hou et al. (2014) and Tijsseling et al. (2016). The focus of the current paper is on (partly) closed dead ends holding entrapped air.

Closed end with entrapped gas pocket

The simplest set of equations describing slug velocity v, front position x_1, and absolute gas pressure P_{gas}, is

$$\frac{\mathrm{d}v}{\mathrm{d}t} = \frac{P_2 - P_{\text{gas}}}{\rho L_0} + g\sin\theta - \frac{f}{2D} v|v| \tag{1}$$

$$\frac{\mathrm{d}x_1}{\mathrm{d}t} = v \tag{2}$$

$$L_{\text{gas}}^n \, P_{\text{gas}} = L_{\text{gas},0}^n \, P_{\text{gas},0} \tag{3}$$

where t is time, P_2 is the upstream driving pressure (absolute), ρ is the liquid density, L_0 is the slug length, g is the gravitational acceleration, θ is the downward angle of inclination of the conduit, f is the skin friction coefficient, D is the inner pipe diameter, n is the polytropic exponent, and L_{gas} is the length of the downstream gas pocket. The subscript 0 indicates initial and constant values. The pressure P_2 can be either constant or variable (as in the experiment). The Eqs. (1)-(3) are solved numerically herein, although analytical solutions have been derived by Tijsseling et al. (2017).

Closed-end calculations

The situation sketched in Figure 12 is simulated with the following input parameters: pipe length (from valve to closed end) $L = 13.4$ m, $D = 0.1$ m, $\theta = -4.6° = -0.08$ rad, $L_0 = m_{\text{slug}} / (\rho A) = 3.1$ m, $\rho = 1000$ kg/m^3, $f = 0.02$, $g = 9.81$ m/s^2 and $n = 1.4$, where $A = 0.00785$ m^2 is the pipe's cross-sectional area and $m_{\text{slug}} = 24$ kg. Upstream driving gas: fictitious length $L_{\text{gas},0} = V_{\text{tank}}/A = 0.5$ m^3/$A = 63.7$ m, $P_{\text{gas},0} = 4$ bar (absolute). Downstream entrapped gas: $P_{\text{gas},0} = 1$ bar (absolute) and $L_{\text{gas},0} = L - L_0 - L_v = 9.65$ m, where $L_v = 0.65$ m is the measured length of the vertical section between valve and upstream initial slug surface, see Figure 1. In Figure 12, $x_L = (63.7 - 0.65)$ (fictitious tank) + 13.4 (pipe) = 76.45 m. The initial slug front is at $x_{1,0} = 63.7 + 3.1 = 66.8$ m and initial velocity $v_0 = 0$.

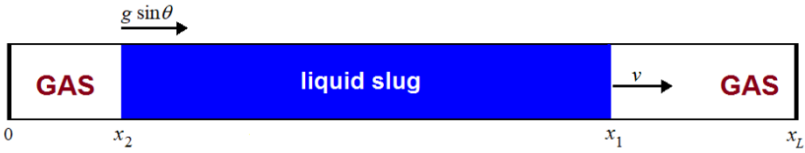

Figure 12. Sketch of extended Bagnold model (not to scale) (Tijsseling et al., 2017)

The instantaneous opening of the valve causes a nearly constant acceleration of the liquid slug until it is impeded and stopped by the compressed air entrapped at the closed end. This behaviour is seen from the slug velocity in Figure 13. The corresponding pressures (upstream and downstream) are displayed in Figure 14. Negative velocity means that the liquid slug has been bounced back by the compressed air. The big question is whether the back-flowing slug is still piston-like or that it is broken up. More striking is that the corresponding experimental result in Figure 5 shows completely different and unexplainable behaviour. The calculated impact pressure in Figure 14 is much more similar to the experimental result of Figure 7, where venting through a 10 mm orifice took place.

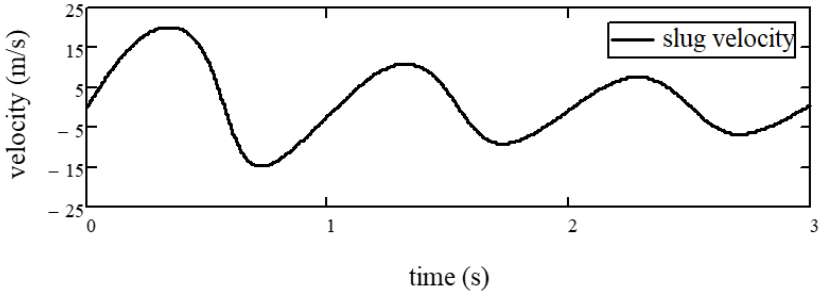

Figure 13. Calculated liquid slug velocity vs. time for 24 kg slug (P_{tank} = 3 bar, closed end)

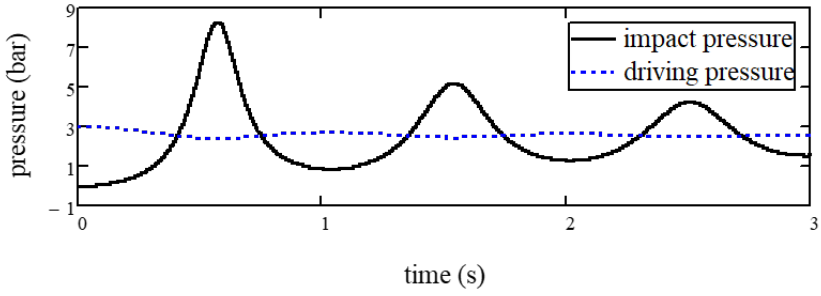

Figure 14. Calculated gas pressures vs. time for 24 kg slug (P_{tank} = 3 bar, closed end)

Orifice end with venting gas pocket

The model of Martin (1976) as explored by Tijsseling et al. (2019) has been used to simulate the experiments with orifice. Figures 15 and 16 show the pressures calculated for 5 mm and 10 mm orifices, respectively, relative to the calculated closed-end pressure. The calculation for the 10 mm orifice stops after 1.7 seconds, because 95% of the air has been expelled. Although Figure 16 shows similarity with the corresponding measurement in Figure 7, it is clear that the current model is too basic to describe the dynamics of the system. Rapid slug break-down seems the most obvious reason.

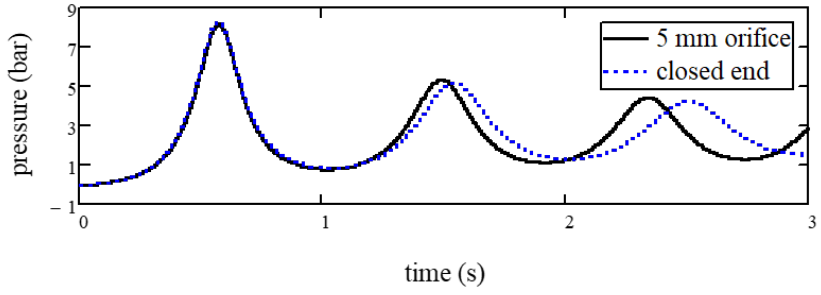

Figure 15. Calculated gas pressures vs. time for 24 kg slug (P_{tank} = 3 bar, 5 mm orifice)

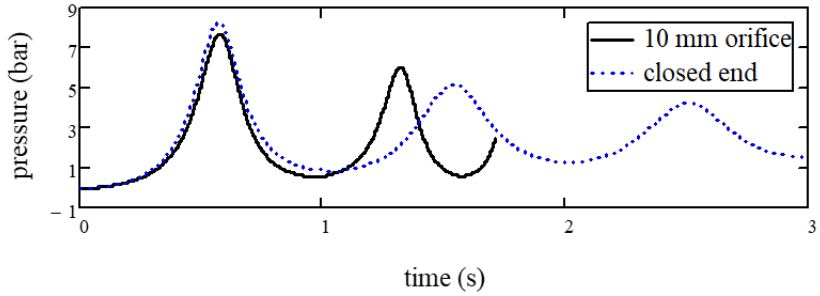

Figure 16. Calculated gas pressures vs. time for 24 kg slug (P_{tank} = 3 bar, 10 mm orifice)

4 CONCLUSION

Novel exploratory slug-impact experiments with entrapped air pockets, venting and non-venting, have revealed a range of issues that need attention. Piston-type slug models cannot fully explain the experimental results. Nevertheless, high peak pressures and oscillatory behaviour have been predicted and observed.

ACKNOWLEDGMENTS

The authors express their gratitude for the financial support offered by the Middle East Technical University Scientific Research Project Program with the project code BAP-03-03-2017-002. The third author participated in the SLING (Sloshing of Liquefied Natural Gas) project, which was funded by STW, MARIN, GTT, and eleven other companies and institutes. In relation to SLING, the authors thank MARIN (Maritime Research Institute Netherlands) for providing technical assistance in the experiments; in particular Hannes Bogaert and Ronnie van Ginkel are thanked for their encouraging attitude.

REFERENCES

Bozkuş, Z., 1991, "The Hydrodynamics of an Individual Transient Liquid Slug in a Voided Line", Ph.D. thesis, Michigan State University, East Lansing, MI, United States.

Bozkuş, Z., Baran, O. U., and Ger, M., 2004, "Experimental and Numerical Analysis of Transient Liquid Slug Motion in a Voided Line", ASME J. Pressure Vessel Technol., 126(2), pp. 241–249.

Dinçer, A. E., 2017, "Numerical Investigation of Free Surface and Pipe Flow Problems by Smoothed Particle Hydrodynamics", Ph.D. thesis, Middle East Technical University, Ankara, Turkey.

Dinçer, A. E., Bozkuş, Z. and Tijsseling, A. S., 2018, "Prediction of Pressure Variation at an Elbow subsequent to a Liquid Slug Impact by using Smoothed Particle Hydrodynamics", ASME J. Pressure Vessel Technol., 140(3), art. no. 031303, (doi:10.1115/1.4039696)

Fenton, R. M., and Griffith, P., 1990, "The Force at a Pipe Bend due to the Clearing of Water Trapped Upstream", Transient Thermal Hydraulics and Resulting Loads on Vessel and Piping Systems, ASME, PVP190, pp. 59–67.

Goyder, H., 2007, "Gas Waterhammer", Proceedings of the ASME Pressure Vessels and Piping Division Conference, San Antonio, USA, Paper PVP2007-26199, pp. 383–390.

Hashimoto, K., Imaeda, M., and Osayama A., 1988, “Transients of Fluid Lines containing an Air Pocket or Liquid Column”, Journal of Fluid Control 18(4), pp. 38–54.

Hatcher, T. M., and Vasconcelos, J. G., 2017, “Peak Pressure Surges and Pressure Damping following Sudden Air Pocket Compression”, Journal of Hydraulic Engineering, 143(4), art. no. 04016094.

Hou, Q., Tijsseling, A. S. and Bozkuş, Z., 2014 “Dynamic Force on an Elbow caused by a Traveling Liquid Slug”, ASME J. Pressure Vessel Technol., 136(3), art. no. 031302, (doi:10.1115/1.4026276).

Kayhan, B. A., and Bozkuş, Z., 2011, “A New Method for Prediction of the Transient Force Generated by a Liquid Slug Impact on an Elbow of an Initially Voided Line”, ASME J. Pressure Vessel Technol., 133(2), art. no. 021701.

Korzilius, S. P., Tijsseling, A. S., Bozkuş, Z., Anthonissen, M. J. H. and Schilders, W. H. A, 2017, “Modelling Liquid Slugs Accelerating in Inclined Conduits”, ASME J. Pressure Vessel Technol., 139(6), art. no. 061301, (doi:10.1115/1.4037716)

Martin, C. S., 1976, “Entrapped Air in Pipelines”, BHRA Fluid Engineering, Proceedings of the Second International Conference on Pressure Surges, London, UK, Paper F2, pp. 15–28.

Owen, I., and Hussein, I. B., 1994, “The Propulsion of an Isolated Slug through a Pipe and the Forces Produced as It Impacts Upon an Orifice Plate”, Int. J. Multiphase Flow, 20(3), pp. 659–666.

Tijsseling, A. S., Hou, Q., and Bozkuş, Z., 2016 “An Improved 1D Model for Liquid Slugs Traveling in Pipelines”, ASME J. Pressure Vessel Technol., 138(1), art. no. 011301, (doi: 10.1115/1.4029794).

Tijsseling, A. S., Hou, Q., and Bozkuş, Z., 2017, “Analytical Solutions for Liquid Slugs and Pigs traveling in Pipelines with Entrapped Gas”, Proceedings of the ASME 2017 Pressure Vessels and Piping Division Conference, Waikoloa, Hawaii, United States, Paper PVP2017-65755.

Tijsseling, A. S., Hou, Q., and Bozkuş, Z., 2019, “Rapid Liquid Filling of a Pipe with Venting Entrapped Gas: Analytical and Numerical Solutions”, ASME J. Pressure Vessel Technol., 141(4), art. no. 041301.

Vasconcelos, J. G., and Leite, G. M., 2012, “Pressure Surges following Sudden Air Pocket Entrapment in Storm-Water Tunnels”, Journal of Hydraulic Engineering, 138(12), pp. 1081–1089.

Yang, J., and Wiggert, D. C., 1998, “Analysis of Liquid Slug Motion in a Voided Line”, ASME J. Pressure Vessel Technol., 120(1), pp. 74–80.

APPENDIX Pressure signal reconstruction

(Such a reconstruction applies to all “too slow” signals recorded by piezoelectric sensors.)

The two PCB (ICP111A26) pressure transducers (A and B) were calibrated by applying a step load (in a separate set-up) as input and obtaining the voltage as output. The results are shown in Fig. A1. The linear regressions shown in the figures were directly entered into the data acquisition system. An example of load relaxation (drifting) of the transducers is given in Fig. A2, where the pressure jumps used for the calibration of transducers A and B are 3.25 bar and 3.1 bar, respectively. One transducer loses its constant load within 2

seconds and the other within 50 seconds. This is the well-known drift behaviour of piezoelectric sensors.

The pipe system in Fig. 1 was also tested with a closed end and air only. The sudden opening of the ball valve caused air-hammer (Goyder, 2007), the typical results of which are shown in Fig. A3. Because of the closed system, there is remaining gauge pressure: 1.6, 2.3, 3.0, 3.8 and 4.5 bar for initial tank pressures of 2, 3, 4, 5 and 6 bar, respectively, measured with a manometer on the air tank [Fig. A3(f)]. This list of remaining (or final) pressures, p_{fm}, is in good approximation a linear function of the initial (jump or peak) pressure p_0, i.e., of the form: $p_{fm} = P_{fm}\, p_0$, where P_{fm} is a constant parameter independent of p_0. Here $P_{fm} \approx 0.8$ is tank volume divided by volume of tank plus pipe. Figure A3(a) shows 17.5 oscillations within a time span of 2.7 seconds, which gives a period $T = 0.154$ s. The pipe length L =13.4 m. The estimated wave speed is $c = 4L/T = 348$ m/s, which is about the speed of sound in dry air at room temperature (the latter not recorded during the tests). The angular frequency of the oscillation (free vibration) is $\omega = 2\pi/T = 40.8$ rad/s.

The issue is that – due to drifting – the PCBs go too low and do not record the remaining (final) gauge pressures. Two Kistler (601C) pressure transducers provided by MARIN (Wageningen) – used as a check – showed the same behaviour. In some tests negative absolute air pressures were measured, which is non-physical, that is impossible. Thus, a justifiable reconstruction is needed.

To reconstruct pressure signals without drifting, the procedure described in this Appendix has been applied. Knowing the shape of the response to a step load (Fig. A2) and/or the final pressure, p_f, in the air-hammer tests (Fig. A3), the original signal can be reconstructed by means of a convolution. The key assumption is that the pressure transducer is a linear input-output system (as confirmed by Fig. A1).

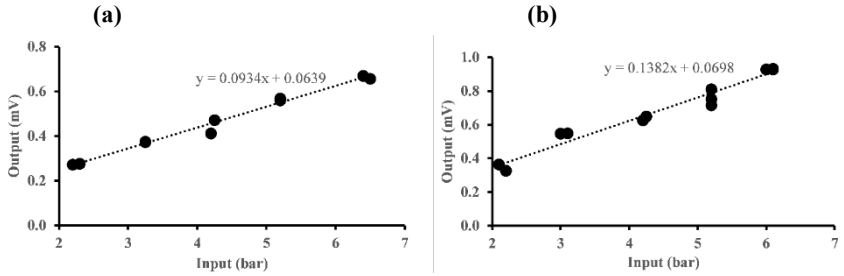

Figure A1. Calibration curve of (a) transducer A and (b) transducer B.

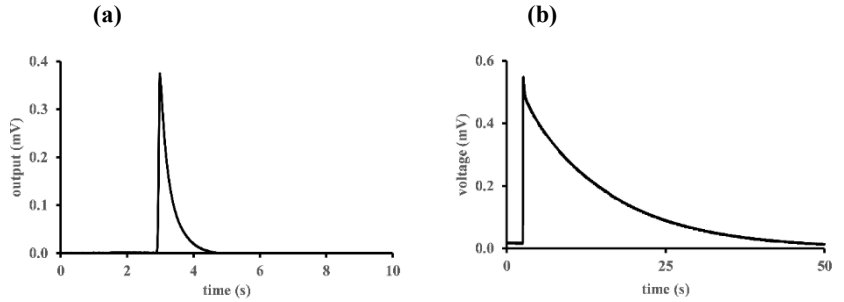

Figure A2. Response to step load of (a) 3.25 bar for transducer A and (b) 3.1 bar for transducer B.

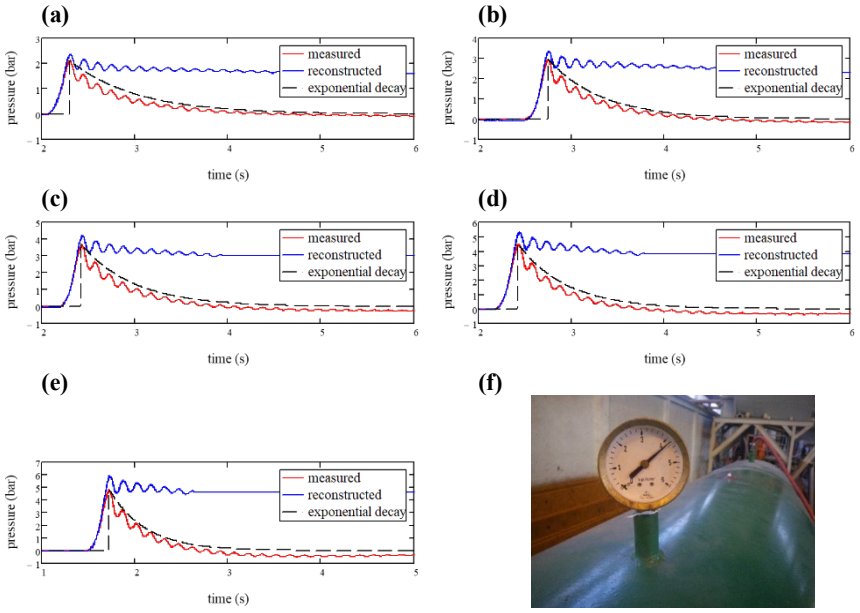

Figure A3. Air-hammer test with closed end for an initial tank pressure (gauge), p_{tank}, of (a) 2 bar, (b) 3 bar, (c) 4 bar, (d) 5 bar, (e) 6 bar, and (f) manometer on air tank showing final pressure (not recorded by pressure transducer A located at the elbow). Reconstruction parameter λ in Eq. (A11b) is (a) 1.40 Hz, (b) 1.73 Hz, (c) 1.77 Hz, (d) 1.93 Hz, (e) 2.56 Hz.

Basic model

We assume that the pressure transducer can be considered as a linear system and that the transfer from measured to real data can be described by a linear integral equation. Let $p_m(t)$ be the measured pressure as function of time t (say $e^{-\lambda(t)}$ in Fig. A2) and $p_r(t)$ the real pressure (say constant 1 in Fig. A2), and let them be related to each other via a linear response relation in which $G(t)$ and $F(t)$ are the response functions. These relations read

$$\int_0^t G(t-\tau)\, p_m(\tau)\, \mathrm{d}\tau = p_r(t) \quad \Leftrightarrow \quad \int_0^t F(t-\tau)\, p_r(\tau)\, \mathrm{d}\tau = p_m(t)\,, \quad t \geq 0. \qquad \text{(A1)}$$

The response functions $G(t)$ and $F(t)$ are specific for the pressure transducer and thus identical for all tests with the same transducer (where, per test, $p_m(t)$ and $p_r(t)$ are different). Hence, the response functions can be derived from a calibration process in which both $p_m(t)$ and $p_r(t)$ are known. Once this has been done, the result can be used in all the performed tests in which only the measured signal $p_m(t)$ is given data. The functions $p_m(t)$ and $p_r(t)$ used for calibration are 0 for $0 < t < t_1$ and show – ideally – a sudden jump of magnitude $p_0 > 0$ at $t = t_1$. This brings us to the assumption that the response functions $G(t)$ and $F(t)$ contain a singular part with a Dirac-delta function $\delta(t)$ and a regular, finite, part. Therefore, let us try

$$G(t) = G_0\, \delta(t) + G_1(t) \quad \text{and} \quad F(t) = F_0\, \delta(t) + F_1(t)\,, \quad t \geq 0, \qquad \text{(A2)}$$

where $G_1(t)$ and $F_1(t)$ are the regular parts, while G_0 and F_0 are constants. Substituting this into (A1), and using that $p_m(t)$ and $p_r(t)$ are 0 for $0 < t < t_1$, we obtain

$$G_0\, p_m(t) + \int_{t_1}^{t} G_1(t-\tau)\, p_m(\tau)\, \mathrm{d}\tau = p_r(t) \quad \Leftrightarrow$$

$$F_0\, p_r(t) + \int_{t_1}^{t} F_1(t-\tau)\, p_r(\tau)\, \mathrm{d}\tau = p_m(t)\,, \quad t > t_1. \tag{A3}$$

Taking the limit $t \downarrow t_1$ of the two relations in (A3), and using that $p_m(t_1) = p_r(t_1) = p_0$, we find that $G_0 = F_0 = 1$. That G_0 and F_0 are unequal to zero confirms the decomposition (A2). With $p_m(t)$ and $p_r(t)$ known, from the calibration tests, we can calculate the response function $G(t)$ (which determines the reconstruction) from the first equation of (A3). Analogously, $F(t)$ can be solved from the second equation of (A3).

Calibration process

In the standard calibration process of Fig. A2, the pressure functions $p_m(t)$ (measured pressure) and $p_r(t)$ (real pressure) are known, where $p_r(t)$ describes a pressure step at time $t = t_1 > 0$ from 0 to p_0, meaning that $p_r(t) = p_0\,\mathrm{H}(t - t_1) = p_0$, for $t > t_1$, with H the Heaviside function. Consequently, the response $p_m(t)$, which is 0 for $t < t_1$, has an identical jump at t_1 and behaves after this time as measured in the test. With all this, we can determine $G_1(t)$ from the first equation of (A3), with $G_0 = 1$, here written as

$$\int_{t_1}^{t} G_1(t-\tau)\, p_m(\tau)\, \mathrm{d}\tau = p_0 - p_m(t)\,, \quad t > t_1. \tag{A4}$$

The Volterra integral equation (A4) can be solved for $G_1(t)$ numerically, for instance by discretisation, noting that measured responses $p_m(t)$ usually are in discrete (sampled) form (see paragraph below). Analogously, we get from the second equation of (A3) for $F_1(t)$, with $F_0 = 1$, the relation

$$p_0 \int_{t_1}^{t} F_1(t-\tau)\, \mathrm{d}\tau = p_0 \int_{0}^{t-t_1} F_1(\tau)\, \mathrm{d}\tau = p_m(t) - p_0\,, \quad t > t_1, \tag{A5}$$

This equation can directly be solved by differentiating it and leads to

$$F_1(t - t_1) = p'_m(t)/p_0\,, \quad t > t_1 \quad \Leftrightarrow \quad F_1(t) = p'_m(t + t_1)/p_0\,, \quad t > 0 \tag{A6}$$

with p'_m the derivative of p_m. For the actual calibration process, we assume that we may approximate $p_m(t)$ by a decreasing exponential function, according to $p_m(t) = p_0\, \mathrm{e}^{-\lambda(t-t_1)}$ for $t > t_1$, with λ a positive constant. In this case, for $p_0 = 1$, (A4) becomes

$$\int_{t_1}^{t} G_1(t-\tau)\, \mathrm{e}^{-\lambda(t-t_1)}\, \mathrm{d}\tau = 1 - \mathrm{e}^{-\lambda(t-t_1)}\,, \quad t > t_1. \tag{A7}$$

This equation can directly be solved (check by substitution), yielding

$$G_1(t) = \lambda\,, \quad t > 0. \tag{A8}$$

From (A6), it follows that

$$F_1(t) = -\lambda\, \mathrm{e}^{-\lambda t}\,, \quad t > 0. \tag{A9}$$

Actual process

In the actual reconstruction process, $p_m(t)$ is given (as a measured sampled data set) and the real pressure $p_r(t)$ is unknown but can be recovered from the first equation of (A3). With $G_0 = 1$ and $G_1(t) = \lambda$, as obtained above, we get

$$p_r(t) = p_m(t) + \lambda \int_{t_1}^{t} p_m(\tau)\, \mathrm{d}\tau\,, \quad t > t_1 > 0. \tag{A10}$$

In basic discretised form, with $t = t_i$, time step Δt, and t_1 properly selected, (A10) reads

$$p_r(t_i) = p_m(t_i) + \lambda \Delta t \sum_{j=1}^{i-1} p_m(t_j)\,, \quad i = 1, 2, 3, \ldots\,, \tag{A11a}$$

so that $p_r(t_1) = p_m(t_1)$ and

$$p_r(t_{i+1}) = p_r(t_i) - p_m(t_i) + (1 + \lambda \Delta t)\, p_m(t_{i+1})\,, \quad i = 1, 2, 3, \ldots\,. \tag{A11b}$$

The value of λ can be estimated either from the measured responses in Fig. A2 or from those in Fig. A3. In this Appendix we have chosen to use Fig. A3 and tune λ such that the final pressure, p_{fr}, in the reconstructed signal matches the value, p_{fm}, shown by the manometer [Fig. 3(f)]. The obtained value of λ is in the range 1.4 to 2.6 Hz (see Fig. A3). However, for the reconstruction of the signals presented in Figs 4-9 we have taken the value $\lambda = 4$ Hz. This larger value was needed to prevent negative absolute pressures.

Illustration

The reconstruction procedure is illustrated and verified by an analytical example. Say, the response of the pressure transducer to a unit step load is an exponential decay, see Fig. A2. Then, the corresponding response function is $G_1(t) = \lambda$ with $G_0 = 1$. Suppose the to-be-reconstructed signal is $p_m(t) = \mathrm{e}^{-\lambda(t)} \cos(\omega t)$ starting at $t_1 = 0$ with $p_0 = 1$, oscillating, and vanishing for large time t, mimicking Fig. 7. The non-vanishing reconstructed signal is, from (A3),

$$p_r(t) = p_m(t) + \int_0^t G_1(t-\tau)\, p_m(\tau)\, \mathrm{d}\tau = p_m(t) + \lambda P_m(t) =$$

$$= p_m(t) + \int_0^t \lambda\, \mathrm{e}^{-\lambda t} \cos(\omega t)\, \mathrm{d}\tau = \mathrm{e}^{-\lambda t} \cos(\omega t) + \frac{\lambda^2 - \lambda^2\, \mathrm{e}^{-\lambda t} \cos(\omega t) + \lambda\, \omega\, \mathrm{e}^{-\lambda t} \sin(\omega t)}{\lambda^2 + \omega^2} \tag{A.12}$$

where P_m is the anti-derivative of p_m. For $\omega = 0$, this reconstructs the constant 1, $t > 0$, see Fig, A4(a). For $\omega > 0$, this gives Fig. A4(b). The limit for $t \to \infty$ of $p_r(t)$ is $p_{fr} = 1/(1+(\omega/\lambda)^2)$. Thus, for high-frequency signals ($\omega/\lambda >> 1$) the reconstruction is not needed, because the dynamic pressure transducer can "handle" it.

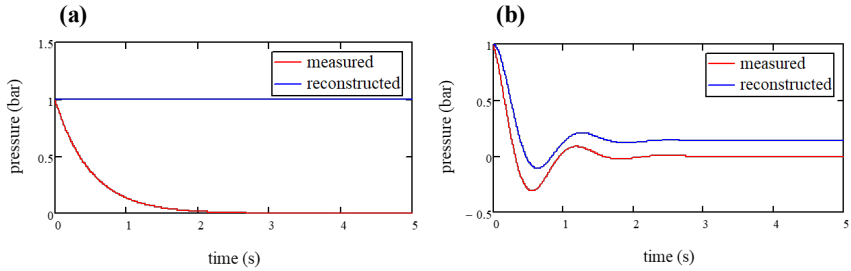

Figure A4. (a) Standard calibration curve and reconstructed signal ($\lambda = 2$, $\omega = 0$), (b) Typical measured signal and its reconstruction ($\lambda = 2$, $\omega = 5$).